J. Agr. Sci. Tech. (2023) Vol. 25(2): 485-502

Improving Soil Texture Digital Mapping Using Landsat 8 Satellite Imageries in Calcareous Soils of Southern Iran

M. Pouzesh Shirazi[1], S. A. Abtahi[1*], M. Bagher Nejad[1], A. A. Moosavi[1], and M. N. Navidi[2]

ABSTRACT

Over the last three decades, there has been a general tendency for changing research methods on soil resource management from conventional and mainly qualitative methods to quantitative ones based on spatial correlation models, which are called Digital Soil Mapping (DSM). The present study was carried out in Shabankareh Plain (15,000 ha) with different physiographic units, in Bushehr Province, southern Iran. The target sites (172 points) were selected for soil sampling at depths of 0-30 cm. Soil texture classes DSM was produced by two methods. The first method was Conventional DSM, in which data of soil particles was obtained from laboratory analysis for each sampling point along with their geographical location. Also, the study area boundary was added to ArcGIS software in UTM format and was analyzed by operating Kriging or IDW estimators. The map produced by this method was a low quality digital map containing extra and scattered texture classes with unrealistically sharp boundaries. The second method used CoKriging of L8 multispectral imagery data (OLI bands) and soil samples analysis was operated. Results showed that using B1 band (0.433-0.453 µm) of Landsat 8 satellite imageries of the study area in April 2020 produced high quality digital maps. In this method, soil textures were the same as the ones in the study area. Salt accumulation and water content of surface soil were possible reasons indicating why satellite imageries in the other periods of year were not suitable for DSM. The highest and the lowest ranges of influence among soil texture parameters were 684 meters and 388 meter for clay and sand particles, respectively.

Keywords: CoKrigging, Geostatistical methods, Reflectance B1band, Soil particle zoning.

INTRODUCTION

Physical and climatic characteristics and unsustainable land management would result in land degradation, which is a significant global phenomenon, particularly in the arid, semi-arid, and semi-humid terrestrial ecosystem environments, and decreas es soil quality and functionality of soil capacity (Turan *et al*., 2019). Soil texture has a great impact on agricultural production and farm management, and is an important physical property that greatly affects other soil properties (Ahmed and Iqbal, 2014). Sufficient information on soil texture in large areas is a requirement for various professionals including soil science engineers, land use managers, cultivation pattern designers, land irritability assessment experts, watershed managers, and even ordinary farmers (Rossiter, 2005). The increasing need for soil properties information on small scales has made conventional laboratory methods seem inadequate. High cost of these methods have resulted in consideration of geostatistical models application, which have the ability of providing a large amount of information as

[1] Department of Soil Science, School of Agriculture, Shiraz University, Islamic Republic of Iran.
[2] Soil and Water Research Institute, Agricultural Research, Education and Extension Organization (AREEO), Karaj, Islamic Republic of Iran.
[*] Corresponding authors; e-mail: seyedaliabtahi@yahoo.com

[DOI: 10.52547/jast.25.2.485]

an alternative to laboratory soil analysis (Manchanda, 2002). Mostly, the high cost of soil studies would demand huge funds; thus, most institutions do not have enough funding to implement these projects. As a result, the tendency to prepare digital soil maps has increased (Robinson *et al*., 2019). In the previous decades, the world soil map was limited to only one map covering the whole world on a small scale, which was provided by the FAO and UNESCO from 1960 to 1980 (Sanchez, 2009; FAO-UNESCO, 1988). Preparation of soil digital maps with high accuracy does not have a long history. For instance, according to a case study in Australia, it dates back merely to the last two decades. For mapping the physical, chemical, and biological properties of different soils on a global scale, digital soil maps have been converted from a university-based research program to operational outputs (Kidd *et al*. 2020). In a study conducted in the Thatta Tehsil Region of Pakistan with the aim of using satellite imagery to calculate soil texture, 30 topsoil samples were collected and soil textures were determined by hydrometric method. Then, soil texture classes were categorized according to the USDA classification method. To evaluate the relationship between the reflectance values of Landsat8 OLI images and soil variables, the Ordinary Least Squares (OLS) regression analyses were used. The results indicated a significant correlation ($P< 0.01$) between the amount of silt with B2 and B5 bands ($R^2= 0.52$), and the amount of clay with B4 and B6 bands ($R^2= 0.40$) (Khalil *et al.,* 2016). In estimating spatial variations in soil properties, accuracy enhancement would be feasible by simultaneous use of a combination of fuzzy algorithms, geostatistical methods, and remote sensing systems. With the surge of agricultural users' knowledge about changes in soil properties, especially soil texture produced through digital maps, we can manage the proper use of land according to Seyedmohammadi *et al*. (2019).

Investigation of the relationship between reflective bands of satellite sensors and soil properties in the field has been reported by statistical functions (Hong *et al*., 2002). Ahmed and Iqbal (2014), using reflective and thermal bands, used Landsat TM sensor imagery and remote sensing methods to map surface soil texture and carbon content. They used multi-linear regression statistical method for statistical calculations. Another study done by Mondejar and Tongco (2019) provided ArcGIS and QGIS software for digital mapping of soil texture class. Extracted GeoTiffs of sand and clay from ArcGIS were inputs to QGIS to draw soil texture classes of the area under study. Shahriari *et al*. (2019) used remote sensing data including Landsat 8 bands and clay index, GSI, and Brightness Index for prediction of soil components in a floodplain. They concluded that, in producing soil digital maps, using Landsat 8 data, when combined with cokriging, regression kriging and Random Forest models, could provide more accurate results.

This study was carried out in an agricultural plain in southern Iran with the objective to prepare digital soil texture maps using field sampling analysis and geostatistical methods. In addition, we aimed to evaluate Landsat 8 satellite OLI reflective bands and remote sensing methods for determining the degree of improvement in the produced maps and investigation soil texture classes and spatial variations.

MATERIALS AND METHODS

Study Area

This research was carried out in the downstream lands of Rais Ali Delvari Dam in Shabankareh Dashtestan Region of semi-arid Bushehr Province, southern Iran, (50° 04′ 18′′ to 51° 51′ 02′ E and 29° 24′ 30′′ to 29° 29′ 18′′ N (Figure 1), with an area of 15,000 ha, which is mainly used for agriculture. In order to find target points easier, their UTM (Universal Transverse

[DOI: 10.52547/jast.25.2.485]

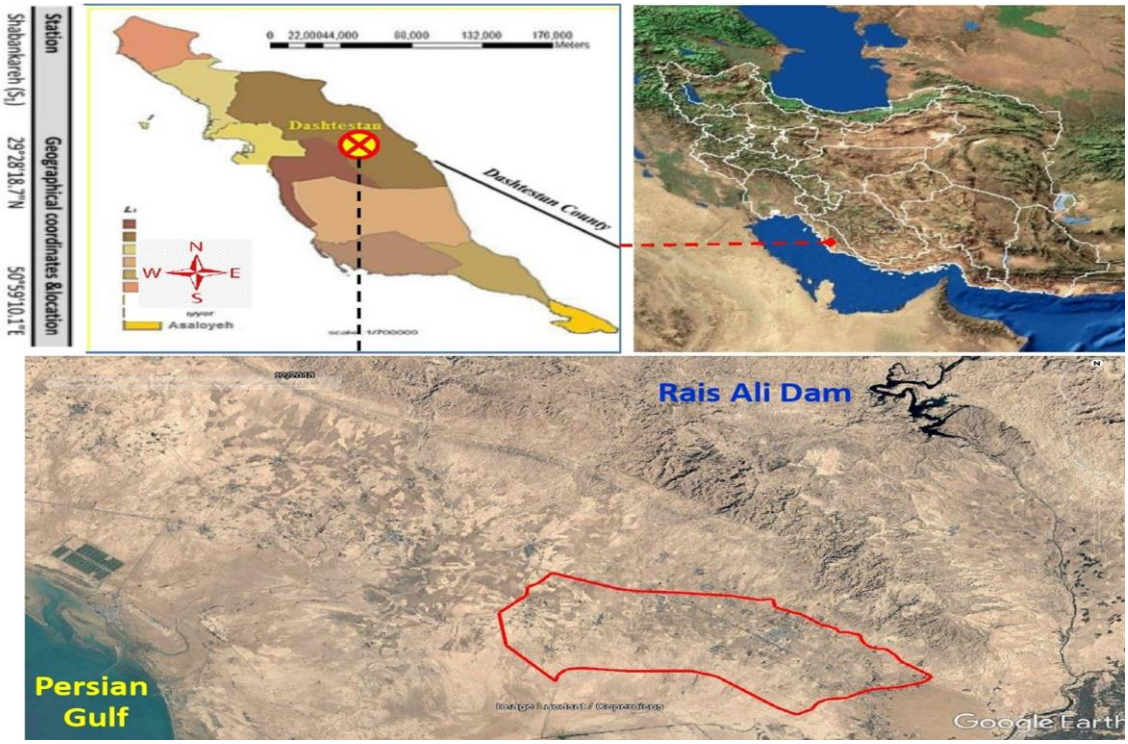

Figure 1. Location of the study area; Dashtestan, Bousher Province, Southern Iran.

Mercator) were added to an application called Area Calculator program in KML format and then soil samples were taken from the study location.

Common crops of the study area include wheat, barley, vegetables, sesame, and canola, which are cultivated in calcareous soil. The region, with an annual mean temperature and precipitation of 24.6°C and 217 mm, respectively (Hyperthermic Aridic), has a hot and dry climate in summer (maximum 54°C) and a moderate climate in winter (minimum 4°C). Agricultural activities mostly occur during the rainy seasons, usually autumn and winter, with moderate climate. The crops, owing to off-season production, have high economic value. Irrigation canals include large reinforced concrete canals with large dimensions and water regulating valves, and are widespread throughout the terrain. Due to the vastness of the study area, there are many types of soils with different physical and chemical properties.

In the starting point, the boundary of the study area was identified on Google Earth satellite imagery. Soil sampling was carried out based on a relatively regular network, according to which more samples were taken in places with a higher density of farms or apparent differences based on close observations. Totally, 172 sampling points were selected (Figure 2).

Five physiographic units were identified in the region owing to their elevations and soil properties consisting of mountains, plateaus, alluvial plains, flood plains and lowlands. As shown in Figure 2, eleven soil profiles were dug for soil survey of the study area.

Soil Taxonomy and Classification

The survey of eleven soil profiles under the latest revision of USDA soil taxonomy expressed by Galbraith *et al*. (2018) was carried out according to the morphological, chemical and physical properties of the profile layers (Figure 3).

[DOI: 10.52547/jast.25.2.485]

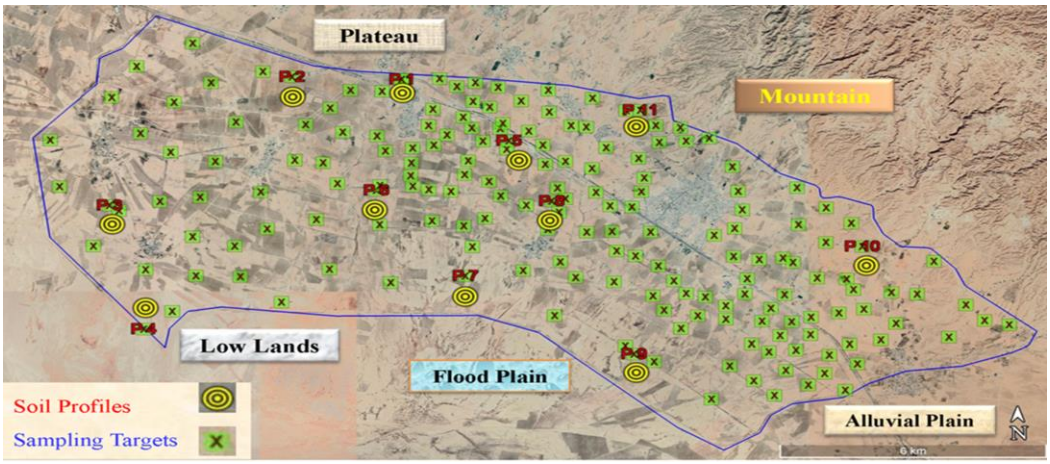

Figure 2. Sampling points and soil profiles in the selected site along with physiographic units.

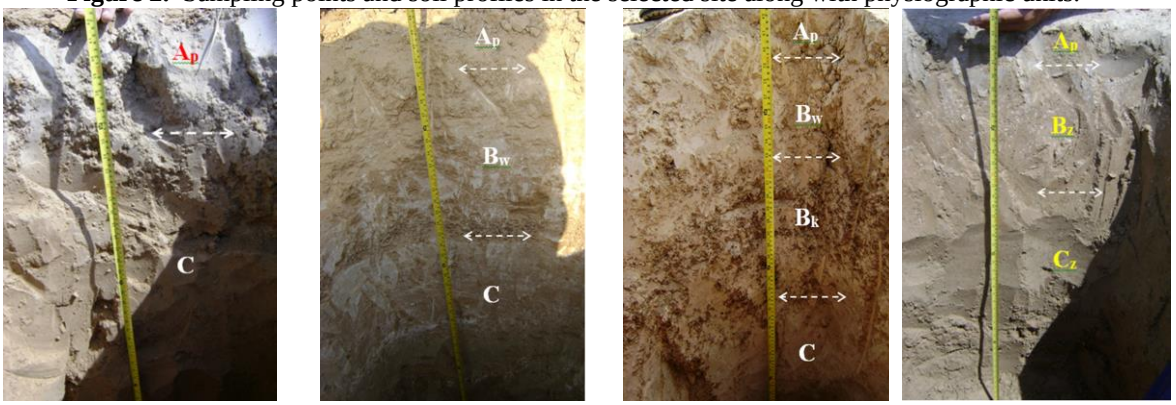

P3: Loamy, mixed, active, calcareous, hyperthermic, Typic Torriorthents

P1: Loamy, mixed, calcareous, hyperthermic, Typic Haplocambids.

P2: Loamy, mixed, active, calcareous, hyperthermic, Typic Haplocalcids.

P4: Loamy, carbonatic, hyperthermic, Typic Aquisalids.

Figure 3. Distinct soil classes observed in the study area with surface appearance.

Two main classes were observed: (a) Entisols; soils located in plateau and higher elevations that were undeveloped, and (b) Aridisols; different families recognized in the study area due to altitude, depositions, calcareous accumulation, water logging and other conditions. Distinct soil classes along with their surface appearances are shown in Figure 3.

[DOI: 10.52547/jast.25.2.485]

Measurement of Soil Texture Components

The hydrometer method was used to determine soil texture; a hydrometer is a device by which the concentration of particles in liquids might be determined. The USDA soil texture triangle was used to determine the texture classes of soils in the area under study, then, the texture classes were drawn by Dplot software.

Digital Elevation Map (DEM)

DEM is a very important map that shows the overall height of the area. Distinctive soil characteristics such as precipitation, types of erosion, leaching of soil particles, type of vegetation, the density of them and lithology are related to the topographic situation (Arabameri *et al*., 2020; Abdollahi *et al*., 2019). The study area was a toposequence from upstream mountains and plateaus with a height of 60 meters toward flood plains and lowlands at sea level. DEM of the study area was prepared from US Geological Survey (USGS Earth Explorer) up to the level of 10 m spatial precision. Then, the map of altitude or hypsometric classes of the study area was generated by Categorize command run by ArcGIS 10.5 software Figure 4.

Statistical Analysis and DSM Mapping

GS^+ software was used to summarize the descriptive statistics of the analyzed soil samples including central statistics and data distribution, skewness, and kurtosis of the data. Logarithmic functions were used to normalize the abnormal data (Ersahin, 2003). This software is based on complex mathematical relationships already obtained from the fitted model over the experimental variogram of a specific variable data (Design, 2004). Data of each sampling point was completely entered in Excel, then, the study of spatial changes of soil texture components was processed by GS^+. For this purpose, the variogram layout of each property was determined initially (Equation 1), then, the anisotropy in the spatial coherence of the data was investigated by determining variogram at different directions.

$$2\gamma(h) = \frac{1}{N(h)} \sum_{i=1}^{N(h)} [z(xi) - z(xi + h)]^2 \quad (1)$$

Where, $2\gamma(h)$ is variogram in distance h, $N(h)$ is the Number of paired samples used

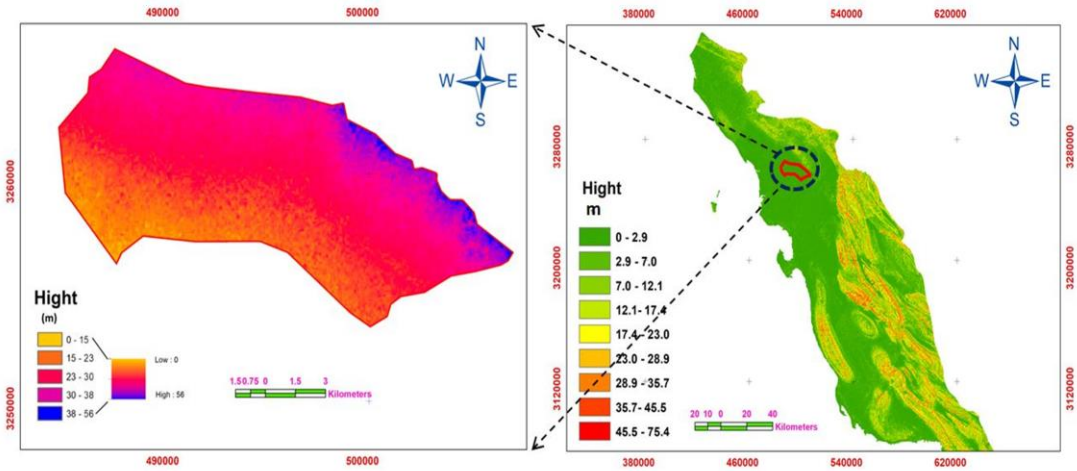

Figure 4. Bushehr Province DEM (right), Elevation classes of study area (left).

[DOI: 10.52547/jast.25.2.485]

to calculate γ(h) at distance h, *z(xi)* is variable value in xi sampling position, and *z(xi + h)* is variable value in the xi+h sampling position

The best experimental model for each character would include the two following properties: (a) The lowest Residual Sum of Square (RSS), which provides a precision measurement of how well the model fits the variogram data, the lower the RSS, the better the model fits data, and (b) The highest R^2, which is an indication of how well the model fits the variogram data. The results achieved from GS^+ were used by ArcGIS 10.5 software to produce DSM outputs. The lowest Root Means Square Error (RMSE) is an important factor for choosing the best estimating method (Kriging or IDW).

Geographical coordinates must be clearly marked in the margins of digital maps, so that it would be possible to find the positions in natural environment easily (Bui, 2020). This capability is available in ArcGIS10.5 software for both UTM or latitude and longitude.

Landsat 8 Satellite imagery

The Landsat 8 satellite was launched in February 2013. Two main sensors of L8 contain Operational Land Imager (OLI) with nine shortwave multispectral bands (0.433 to 1.360 µm) and have two thermal infra-red sensors (10.6 to 12.5 µm). Imagery coverage is 185 km swath and 30 m spatial resolution for all bands except for OLI (panchromatic) and thermal bands with 15 and 100 m resolution, respectively (Li and Chen 2014).

In order to find out the best imagery period for improving texture DSM, L8 imagery path 164, and row 040 were downloaded for all midseason (January, April, July and October) from 2020. In this case, the effects of land coverage by plants and soil moisture or salt accumulation could be eliminated. Pre-processing was applied to download OLI imageries by geometric, atmospheric and radiometric corrections done by ENVI software. The best Atmospheric Correction Method (ACM) was chosen by comparing the Pearson correlations, achieved from SPSS analysis, between soil particles data and two ACM methods.

Conventional and Improved Methods for Digital Mapping of Soil Texture Classes

Methodology framework of the study is shown in Figure 5. In conventional DSM method, data of soil components, obtained from laboratory analysis, along with their geographical location and study area boundary were added to ArcGIS software in UTM format (Zone; 39 R, Datum; WGS84).

GS^+ outputs contain summary statistics, determine isometry of variables, and calculate the range effects of each soil particle, which are valuable data for studying spatial distributions; whereas, produced maps by GS^+ cannot be used as inputs to QGIS software for generating soil textural triangle.

Therefore, ArcGIS software was used to export data to shapefile for operating geostatistical wizard and producing digital maps of soil particles through Kriging or IDW. In the last step, extracted GeoTiffs of soil particles were added to QGIS software for producing soil textural triangle.

In the improved DSM method, soil sampling results were correlated to the reflectance values of Digital Numbers (DN) obtained from Landsat 8 OLI images. The summary of the improved method was as follows: In the improved DSM method, soil sampling results were correlated to the reflectance values of Digital Numbers (DN) obtained from Landsat 8 OLI images. The summary of methodology for improved method was as follows;

A) Imagery treatments: Downloading L8 multispectral imagery data (OLI) from USGS, Pre-processing Dark Subtraction to achieve the best imagine, Resizing 7 Bands to make the boundary of the study area in the center of the image, and eliminating

[DOI: 10.52547/jast.25.2.485]

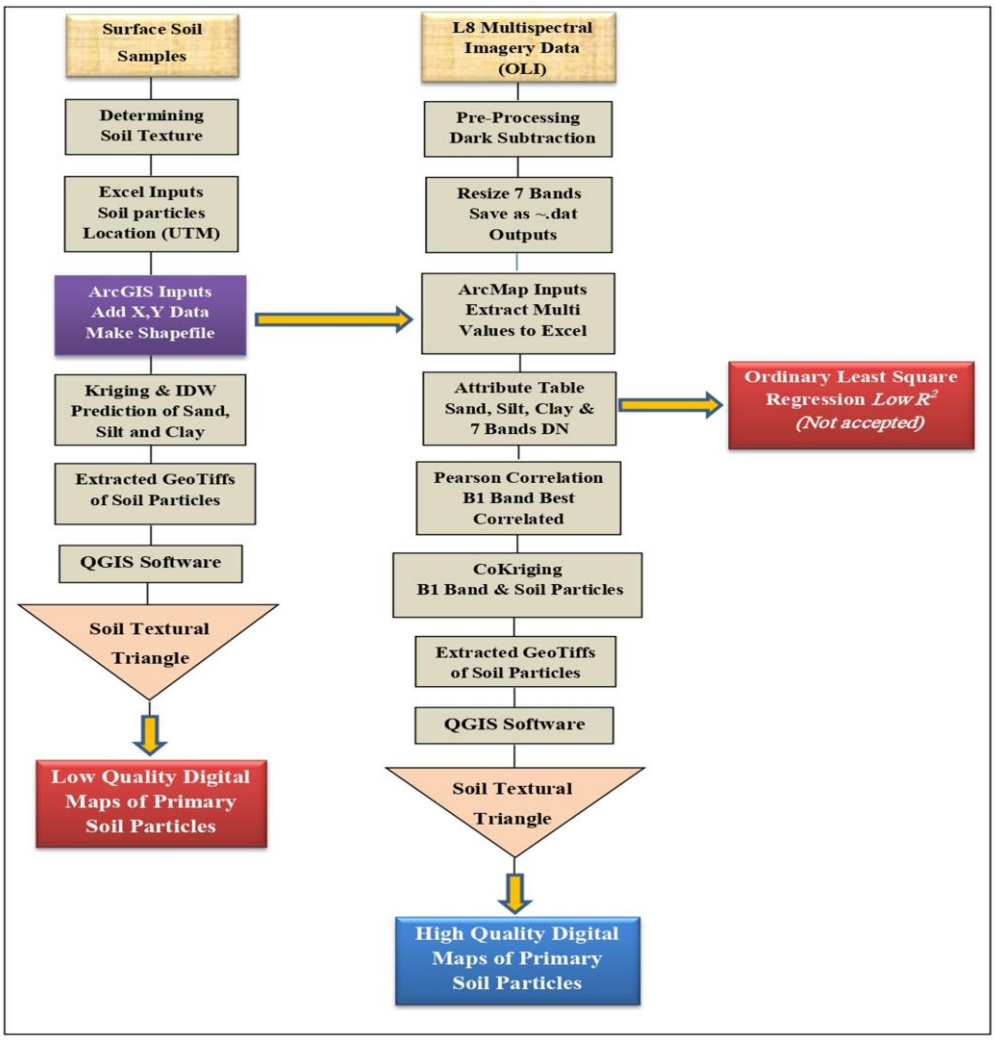

Figure 5. Methodology framework of the study.

extra areas, saving as ~.dat outputs for exporting data to ArcMap environment.

B) ArcGIS operations: Adding X, Y data and making shapefile of the data and study area boundary, ArcMap Inputs from extracted multi values to Excel to collect all the bands in a single file, attributing table sand, silt, clay with 7 bands DN for geostatistical operations.

C) Geostatistical workouts: CoKriging of B1 band and soil particles to estimate values for places with no data of soil particles and decreasing estimation errors, extracted GeoTiffs of soil particles as inputs for QGIS software, producing soil textural triangle by QGIS software, and calculating the area of each soil texture in ArcGIS.

The overall methodology which was adopted in this study for operating digital mapping of soil particles is shown in Fig 5.

RESULUTS AND DISCUSSION

Descriptive Statistics of Data

Soil texture classes determined by Dplot software are shown in Figure 6. Six textural classes were obtained from USDA texture triangle containing Sandy Loam (SL), Loam

[DOI: 10.52547/jast.25.2.485]

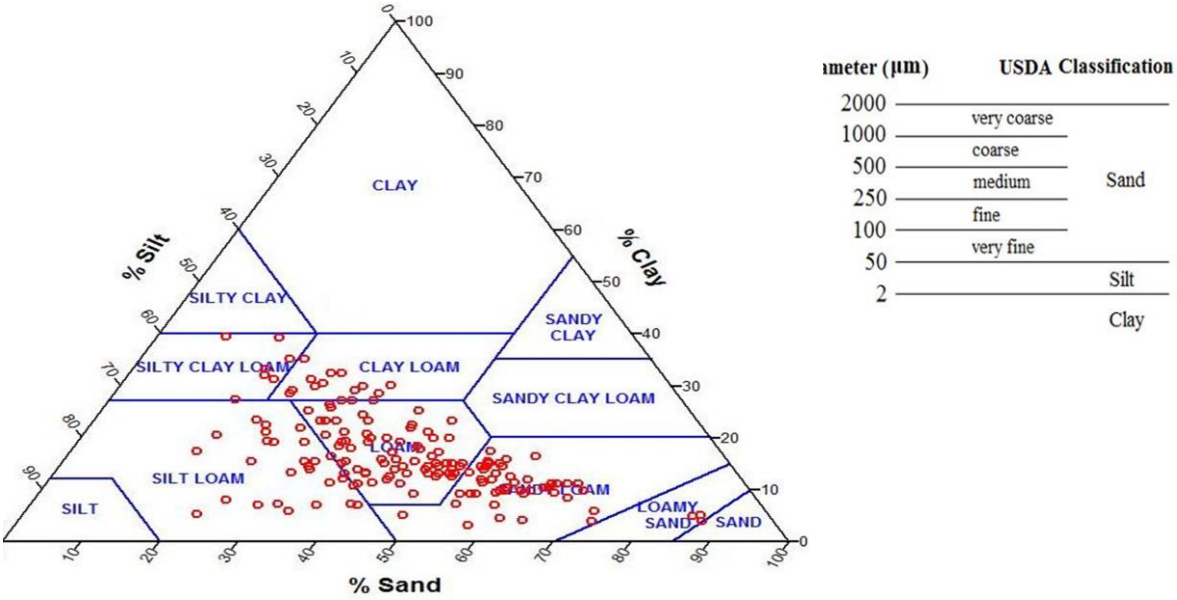

Figure 6. Texture classes of studied soil samples based on USDA texture triangle.

(L), Clay Loam (CL), Silt Loam (SiL), Silty Clay Loam (SiCL), and Loamy Sand (LS) (Figure 6). This indicated that in most parts of the study area, soil texture was medium (loam), which is considered as a desirable texture in agriculture in terms of suitable aeration, supplying plant nutrients, and water holding capacity of the soil. Therefore, due to the existence of a reliable source of water upstream of Rais Ali Delvari Dam, the value of proper land management of Shabankareh Plain is comprehensible.

The summary of descriptive statistics of soil particles data is presented in Table 1. When the textural fractions of soils dominated by the medium texture group were examined, it was revealed that the highest variation coefficient was for Clay (C). Although all soil components showed normal distribution, Silt (Si) and Clay (C) showed the lowest (0.27) and highest (0.47) coefficient of variation among the primary components of soil texture. This difference was in consequence of clay formation changes in soil evolution in the toposequence of the study area. Higher variation coefficient for Clay (C) was reported by Alaboz *et al*. (2020) in Isparta Atabey Plain.

Even though CV alone is not enough to determine the space variability of soil components, compared to other parameters such as SD, mean, and median, it was the most distinctive factor in describing the diversity of soil properties (Xing-Yi *et al*. 2007).

However, the geostatistical analysis would be necessary to determine the spatial

Table 1. Descriptive statistics of data for soil components.

Soil particle	Min	Max	Mean	Std dev	CV[a]	Skew[b]	Kurt[b]	Kol-Smi test[c]
Sand	8.51	86.74	42.21	15.11	0.35	0.33	-0.13	0.20
Silt	8.75	72.72	40.92	10.89	0.27	-0.08	0.44	0.20
Clay	3.34	45.33	16.97	7.99	0.47	0.84	0.52	0.12

[a] Coefficient of Variation values: < 0.1, 0.1-0.2 , 0.2-0.3, > 0.3 (Very low, low , medium and high difference, respectively) . [b] Skewness and Kurtosis: -2< Normal < 2, [c] Kolmograph-Smirnov test: Normal, Sig> 0.05.

[DOI: 10.52547/jast.25.2.485]

Table 2. Summary of geostatistical analysis of the studied properties and theoretical model.

Soil particle	Isotropy/ Anisotropy	Model	Nugget effect (C_0)	Sill ($C+C_0$)	Range (m)	C_0/ C_0+C	R^2	RSS
Sand	Isotropic	Spherical	147.0	464.2	388	0.68	0.92	2401
Silt	Isotropic	Spherical	60.1	299.5	411	0.73	0.93	955
Clay	Anisotropic	Exponential	58.6	160.1	684	0.63	0.57	5581

dependency of soil particles in addition to the statistical analysis (Seyedmohammadi *et al*., 2019). Thus, Kolmograph-Smirnov test was used to check the normal distribution of the studied soil attributes by SPSS, which proved to be normal like skewness and kurtosis results (Vrbik, 2020). In case of abnormal data, logarithmic transformation can be used to normalize data (Robinson and Metternicht, 2006).

Spatial Variations of Soil Texture Components

A summary of geostatistical analysis of the studied attributes and also the best theoretical models fitted to their experimental variograms are shown in Table 2. By considering the maximum coefficient of determination (R^2) and minimum Residual Sums of Squares (RSS), the best experimental models were selected. A higher R^2 of more than 0.5 indicates a strong spatial correlation. Silt had the highest R^2 and lowest RSS, while clay particles had the lowest R^2 and highest RSS. The strengths of the spatial structure of the variables are displayed with the spatial isotropic ratio or (C_0/C_0+C). When this ratio is less than 0.25, the spatial structure is strong, and in case the ratio is between 0.25-0.75 and more than 0.75, it shows the medium to weak structure, respectively (Design, 2004).

The strong and medium spatial structure is related to the inherent factors of the soil as to origin and genesis of soil influenced by parent material; whereas weaker spatial structure indicates the significant effects of external factors such as erosion, sedimentation, or plowing. The strongest spatial structure was related to clay (nugget to sill ratio of 0.63) followed by that of sand (0.68) and silt (0.73) (Cambardella *et al*., 1994). Besides, the highest range of influence was 684 m for clay particles. Maps generated by GS+ software are shown in Figure 7.

GS^+ geostatistical results were used in ArcGIS software for drawing maps (Figure 8). Lower RMSE was the reason for choosing Kriging or IDW estimators in ArcGIS. RMSE values were 7.42, 12.52, and 8.70 for clay, sand, and silt particles all by Kriging model, respectively.

Digital maps drawn by ArcGIS software are more valuable than the maps generated by other software for two reasons. First, the boundary of the study area, as well as geographical coordinates, are clearly visible in the ArcGIS-produced maps; therefore, it is possible to locate the study area in satellite images and field conditions easily, which is considered a very important point in terms of land management. Second, ArcGIS maps might provide more comprehensive and thorough visual information for the researcher and operator; thus, the possibility of using the produced maps by other remote sensing software for supplementary study is available.

Spatial Variation of Soil Texture Classes

According to digital maps drawn by ArcGIS in conventional method, the amount of clay in the western and middle parts of the Shabankareh Plain was more than that in other parts of the study area; whereas higher lands located in the north and west contained more sand particles (Figure 9). Lowlands, as well as sedimentary plains in the southern part of the study area, contained large amounts of silt. These maps can reveal important soil properties such as porosity degree, permeability rate, water holding capacity, fertility, and soil erosion prediction through modeling (Ostovari *et al*., 2021).

[DOI: 10.52547/jast.25.2.485]

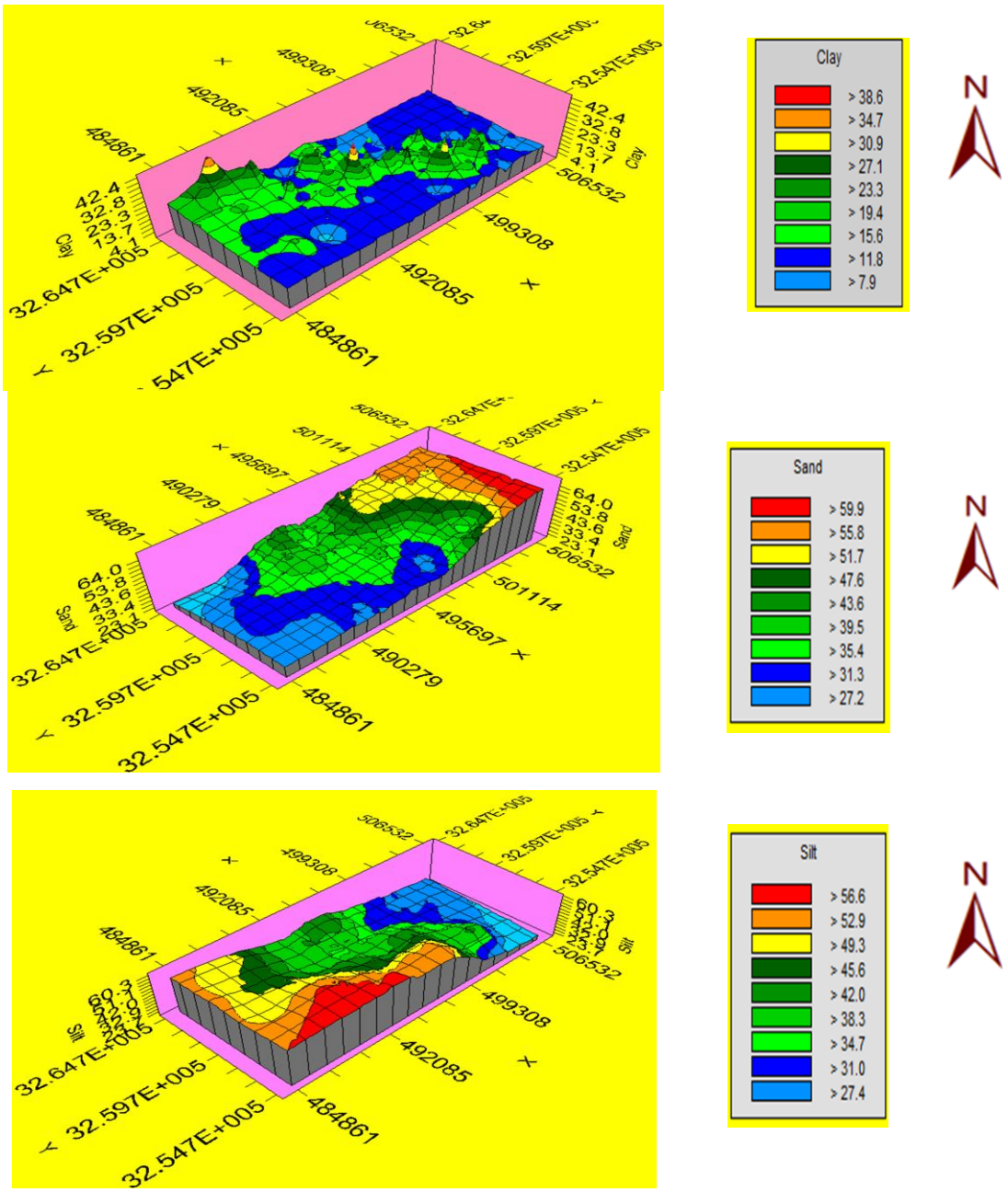

Figure 7. Zoning maps of the Kriged soil particles percent maps using GS$^+$.

In addition, for determining the pattern of plant cultivation, more detailed studies might be performed from DSM maps. For instance, plants that need better drainage conditions can be cultivated in lands with higher sand percentages specified in the map. Also, in areas with large amounts of clay particles, the possibility of floods and transfer of suspended solids can happen more than the other places. In such conditions, the transfer of pollutants and sediments to downstream water sources and land flooding would happen seriously as infiltration rate decreases (Tashayo *et al*. 2020).

[DOI: 10.52547/jast.25.2.485]

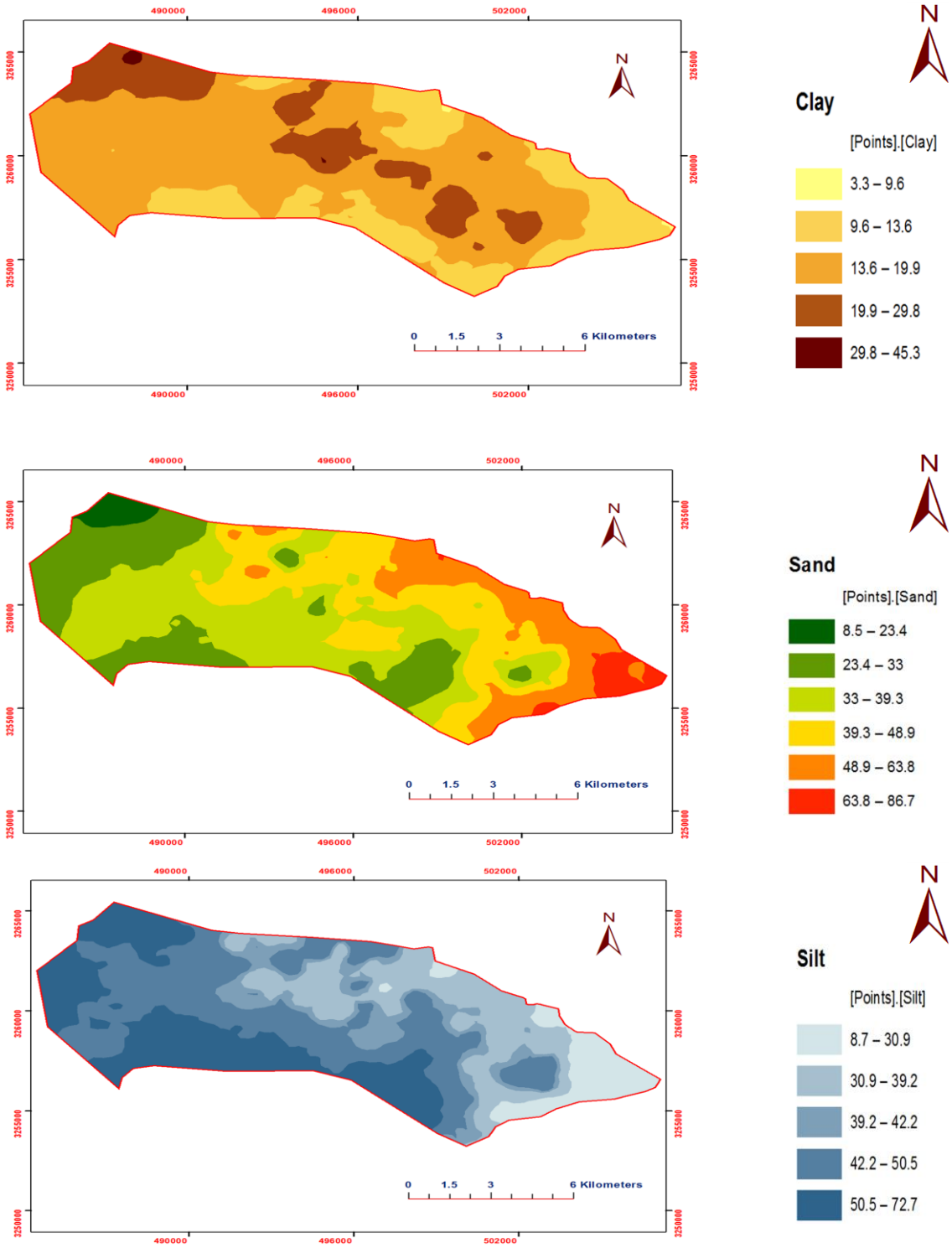

Figure 8. Zoning and digital maps of soil particles produced by ArcGIS.

For digital mapping of soil texture class, use of extracted GeoTiffs of sand and clay in QGIS software was reported by other researchers. Mondejar and Tongco (2019) used the same software to produce digital maps for the surface texture of the Philippines soils.

[DOI: 10.52547/jast.25.2.485]

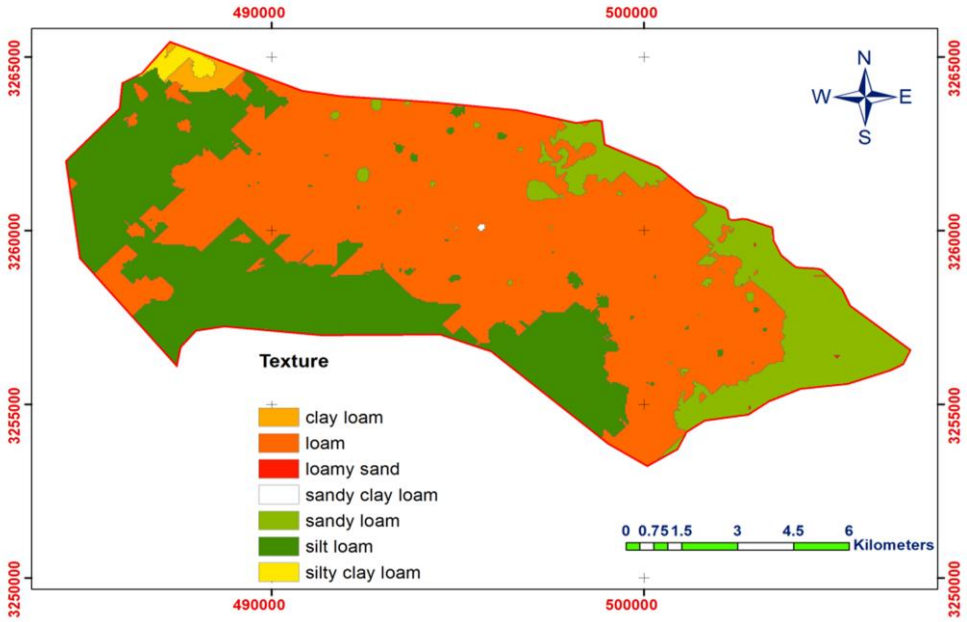

Figure 9. Digital soil texture class map produced by conventional method.

Although conventional method is very common, the digital maps produced by this simple method had a poor quality and resulted in the following three drawbacks:

1). There were six textural classes according to USDA soil texture triangle as shown in Figure 6, while there were seven classes in the map produced by this method. The new extra class was Sandy Clay Loam, which did not exist in the study area.

2). Margin of soil texture classes indicate boundaries with unrealistically sharp edges, a phenomenon that does not normally happen in nature.

3). Soil classes with small areas were scattered throughout the study area, which did not seem logical according to the homogeneity of these soils.

All of the three above drawbacks were due to the inaccuracy of the estimation by the modeling estimators (Kriging and IDW). If the number of soil samples were not adequate, the unwanted drawbacks would occur more often.

To solve the abovementioned problems and improve the quality of digital maps for soil texture class, the use of Landsat 8 (L8) satellite imageries was recommend.

Due to the vastness of the study area, soil survey and sampling lasted for about two months from January to February 2020. Owing to the fact that soil texture was a constant parameter in soil properties, to find out the best time of satellite images for soil particles measurement, L8 imageries were uploaded from USGS Earth Explorer for all 2020 midseasons.

A large amount of data was downloaded. Atmospheric correction was done by Dark subtraction method, DNs of Pre-processing OLI imageries were extracted to the attribute table in ArcGIS. In the next step, Pearson coefficients between satellite bands (B1 to B7) and soil particles were calculated by SPSS for all midseasons as shown in Table 3. The highest correlations between clay and sand (as QGIS inputs for DSM texture classes) and OLI bands were -0.234 and 0.323 with B6 and B7 in January, and -0.305 and 0.211 with just B1 in April, respectively.

The following two methods have been recommended for improving DSM by satellite imageries in different studies:

1) The first and common method is calculating Ordinary Least Squares (OLS)

[DOI: 10.52547/jast.25.2.485]

Table 3. Pearson correlation coefficient matrix for soil properties and L8 OLI bands.

	Particle	Clay	Silt	Sand	B1	B2	B3	B4	B5	B6	B7	
(Winter) Jan 2020	Clay	1.000	0.271	-0.717	**-0.305****	-0.242	-0.213	-0.181	-0.024	-0.161	-0.150	(Spring) April 2020
	Silt	0.271	1.000	-0.863	-0.094	-0.089	-0.060	-0.015	-0.105	-0.147	-0.162**	
	Sand	-0.717	-0.863	1.000	**0.211****	0.191	0.154	0.103	0.095	0.188	0.192	
	B1	-0.133	-0.102	0.150	1.000	0.987	0.971	0.901	0.403	0.861	0.764	
	B2	-0.145	-0.127	0.175	0.994	1.000	0.980	0.945	0.332	0.912	0.832	
	B3	-0.202	-0.151	0.222	0.952	0.972	1.000	0.948	0.417	0.918	0.811	
	B4	-0.193	-0.122	0.197	0.944	0.967	0.986	1.000	0.136	0.949	0.903	
	B5	0.083	-0.029	-0.024	-0.478	-0.487	-0.453	-0.544	1.000	0.217	-0.018	
	B6	**-0.234****	-0.262	0.318	0.730	0.786	0.876	0.873	-0.319	1.000	0.958	
	B7	-0.215	-0.282**	**0.323****	0.775	0.826	0.890	0.898	-0.414	0.979	1.000	
(Summer) July 2020	Clay	1.000	0.271	-0.717	-0.138	-0.117	-0.119	-0.084	-0.066	-0.096	-0.121	(Autumn) Oct 2020
	Silt	0.271	1.000	-0.863	0.215**	0.191	0.146	0.106	-0.061	-0.015	0.120	
	Sand	-0.717	-0.863	1.000	-0.082	-0.076	-0.044	-0.034	0.074	0.057	-0.024	
	B1	**-0.167****	0.334**	-0.154	1.000	0.975	0.904	0.765	0.355	0.593	0.845	
	B2	-0.138	0.327	-0.164	0.971	1.000	0.961	0.870	0.520	0.726	0.884	
	B3	-0.111	0.294	-0.155	0.908	0.973	1.000	0.957	0.672	0.837	0.907	
	B4	-0.084	0.266	-0.150	0.818	0.918	0.979	1.000	0.803	0.929	0.857	
	B5	-0.080	0.128	-0.055	0.536	0.690	0.792	0.853	1.000	0.870	0.516	
	B6	-0.091	0.129	-0.049	0.644	0.780	0.866	0.925	0.888	1.000	0.809	
	B7	-0.114	0.237	-0.112	0.863	0.879	0.879	0.844	0.564	0.785	1.000	

* Correlation is significant at the 0.05 probability level, ** Correlation is significant at the 0.01 probability level.

regression between the selected bands and particles. The regression relationships obtained are shown in Table 4.

R^2 values obtained by (OLS) regression were too small (Table 4). Therefore, practically it was impossible to use these relationships, so, the first method was eliminated.

2) In the second recommended method, Co-Kriging was used between the atmospherically corrected reflectance bands of L8 and soil particles by ArcGIS geostatistical wizard. The results proved that map of soil texture classes produced by B1 band of April 2020, in comparison to maps of B6 and B7 bands, had a higher quality through January 2020. This was mainly due to the less scattered classes, smoother margin boundaries, and no unreal (extra) classes (Figure 10).

The texture classes areas in hectares are shown in Figure 11. No extra texture class was produced in DSM by this method.

In OLI reflectance sensors, B1 band was considered as a coastal aerosol band (0.43-.45 µm) and the soil texture map produced by this band was very similar to the nature of the study area. As a result, it seems that in the regions that are near the sea, as the study area, B1 band of Landsat 8 being extracted in April might be used for producing high quality digital maps of soil particles with no attention to the time of soil sampling (soil sampling was done 3 months before). This shows that using suitable satellite imageries band can help eliminate the estimation errors of geostatistical estimators and produces high quality DSMs.

In the study area, the growth stages started in October and finished in March, i.e. the cultivation season. In April, the topsoil is almost bare, with low moisture and less

[DOI: 10.52547/jast.25.2.485]

Table 4. Regression between soil particles and OLI bands.

January (2021)	R^2	April (2021)	R^2
Clay= 34.334 – 0.001 × B6	0.055	Clay= 80.327 – 0.005 × B1	0.073
Sand= 7.98 + 0.003 × B7	0.104	Sand=-51.173 + 0.008 × B1	0.044

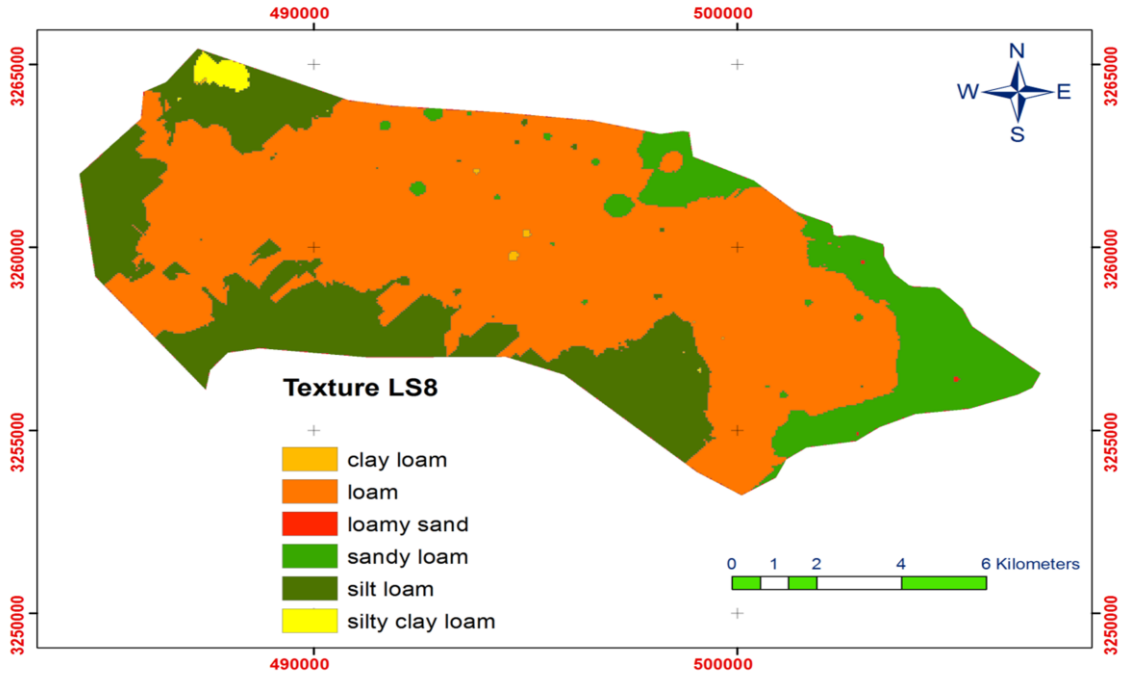

Figure 10. Improved digital map of soil texture classes using B1 band of Landsat 8.

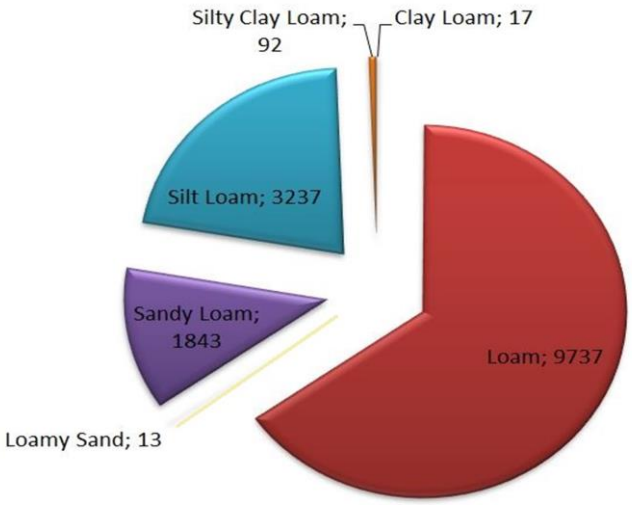

Figure 11. The area of texture classes in the study plain (ha).

[DOI: 10.52547/jast.25.2.485]

plant coverage. In this condition, the best reflectance would be obtained; whereas, high surface soil moisture through winter and also salt accumulation under capillary action during summer are the possible reasons for satellite imageries being unsuitable for DSM of soil texture.

CONCLUSIONS

Application of digital soil maps based on remote sensing is rapidly expanding in in the whole world including Iran. These maps are not only used in precision targeted cultivation but also are useful in extensive global and transnational studies such as world environmental protection and challenging pollutants such as extra-regional dust pollution. The results showed that the strongest spatial textural class was related to soil clay particles (nugget to sill ratio of 0.63) and the weakest one was observed in silt (0.73). Furthermore, among soil texture components, the highest and lowest ranges of influence were 684 m and 388 m for clay and sand, respectively.

Although conventional method is very common in DSM, the soil texture digital maps produced via this simple method were poor in terms of quality, and thus resulted in many scattered areas with both real and unreal (extra) soil classes throughout the study area. Therefore, in areas with specific soil characteristics such as the study area, which is adjacent to the sea, the use of B1 band of L8 satellite imageries is suggested, since it can produce high quality digital maps for primary soil particles. For proper land management, using quality digital maps produced in this research is suggested. For instance, sandy soils with better aeration are located in the north and east parts of the area, and they can be better used for cultivating plants that need proper drainage; while more tolerant plants can be planted in the west and south having heavier soils with more clay. In areas with different land managements, digital maps are useful on both national and global scale.

REFERENCES

1. Abdollahi, S., Pourghasemi, H. R., Ghanbarian, G. A. and Safaeian, R. 2019. Prioritization of Effective Factors in the Occurrence of Land Subsidence and Its Susceptibility Mapping Using an SVM Model and Their Different Kernel Functions. *Bull. Eng. Geol. Environ.,* **78(6):** 4017-4034.
2. Ahmed, Z. and Iqbal, J. 2014. Evaluation of Landsat TM5 Multispectral Data for Automated Mapping of Surface Soil Texture and Organic Matter in GIS. *European J. Remote Sens.,* **47(1):** 557-573.
3. Alaboz, P., Demir, S. and Dengiz, O. 2020. Determination of Spatial Distribution of Soil Moisture Constant Using Different Interpolation Model Case Study, Isparta Atabey Plain. *J. Tekirdag Agric. Fac.,* **17(3):** 432-444.
4. Arabameri, A., Pradhan, B. and Bui, D. T. 2020. Spatial Modelling of Gully Erosion in the Ardib River Watershed Using Three Statistical-Based Techniques. *Catena,* **190:** 104545.
5. Bui, E.N., Searle, R. D., Wilson, P. R., Philip, S. R., Thomas, M., Brough, D. and Van Gool, D. 2020. Soil Surveyor Knowledge in Digital Soil Mapping and Assessment in Australia. *Geoderma Reg.,* **22:** 1-50.
6. Cambardella, C. A., Moorman, T. B., Parkin, T. B., Karlen, D. L., Novak, J. M., Turco, R. F. and Konopka, A. E. 1994. Field-Scale Variability of Soil Properties in Central Iowa Soils. *Soil Sci. Soc. Am. J.,* **58(5):** 1501-1511.
7. Design G. 2004. Geostatistics for the Environmental Science Version 7. Gamma Design, USA, 159 PP.
8. Ersahin S. 2003. Comparing Ordinary Kriging and Cokriging to Estimate Infiltration Rate. *Soil Sci. Soc. Am. J.,* **67(6):** 1848-1855.

[DOI: 10.52547/jast.25.2.485]

9. FAO-UNESCO. 1988. *Soil Map of the World, Revised Legend*. World Soil Resources Report, Rome, 60 PP.
10. Galbraith, J. M., Stolt, M. H., Rabenhorst, M. C. and Ransom, M. D. 2018. Impacts of Fundamental Changes to Soil Taxonomy. *S. Afr. J. Plant Soil*, **35(4):** 263-267.
11. Gee G. W. and Bauder, J. W. 1986. Particle-Size Analysis. Part 1. Agron. WI. Particle-Size Analysis. In: "*Methods of Soil Analysis*", (Ed.): Klute, A. Monogr. 9. ASA and SSSA, Madison, WI, PP. 383–409.
12. Hong S. Y., Sudduth K. A., Kitchen N. R., Drummond S. T., Palm H. L. and Wiebold W. J. 2002. Estimating within-Field Variations in Soil Properties from Airborne Hyperspectral Images. *In Pecora 15/Land Satellite Information IV/ISPRS Commission I/FIEOS 2002 Conference Proceedings*, PP. 1-13.
13. Khalil, R. Z., Khalid, W. and Akram, M. 2016. Estimating of Soil Texture Using Landsat Imagery: A Case Study of Thatta Tehsil, Sindh. *In 2016 IEEE International Geoscience and Remote Sensing Symposium (IGARSS)*, IEEE, PP. 3110-3113.
14. Kidd, D., Searle, R., Grundy, M., McBratney, A., Robinson, N., O'Brien, L. and Jones, E. 2020. Operationalising Digital Soil Mapping–Lessons from Australia. *Geoderma Reg.*, **23:** e00335.
15. Li, S. and Chen, X. 2014. A New Bare-Soil Index for Rapid Mapping Developing Areas Using Landsat 8 Data. Int. *Arch. Photogramm. Remote Sens. Spat. Inf. Sci.*, **40(4):** 139.
16. Manchanda, M. L., Kudrat, M. and Tiwari, A. K. 2002. Soil Survey and Mapping Using Remote Sensing. International Society for Tropical Ecology, **43(1):** 61-74.
17. Mondejar, J. P. and Tongco, A. F. 2019. Estimating Topsoil Texture Fractions by Digital Soil Mapping: A Response to the Long Outdated Soil Map in the Philippines. *Sust. Environ. Res.*, **29(1):** 1-20.
18. Ostovari, Y., Moosavi, A. A., Mozaffari, H. and Pourghasemi, H. R. 2021. RUSLE Model Coupled with RS-GIS for Soil Erosion Evaluation Compared with T Value in Southwest Iran. *Arab. J. Geosci.*, **14(2):** 1-15.
19. Robinson, N. J., Dahlhaus, P. G., Wong, M., MacLeod, A., Jones, D. and Nicholson, C. 2019. Testing the Public–Private Soil Data and Information Sharing Model for Sustainable Soil Management Outcomes. *Soil Use Manag.*, **35(1):** 94-104.
20. Robinson T. P. and Metternicht, G. 2006. Testing the Performance of Spatial Interpolation Techniques for Mapping Soil Properties. *Comput. Electron. Agric.*, **50(2):** 97-108.
21. Rossiter, D. 2005. Digital Soil Mapping; towards a Multiple-Use Soil Information System. *Análisis Geográficos (Revista del Instituto Geográfico" Augusín Codazzi")*, **32(1):** 7-15.
22. Sanchez, P. A., Ahamed, S., Carré, F., Hartemink, A. E., Hempel, J., Huising, J. and Minasny, B. 2009. Digital Soil Map of the World. *Science*, **325(5941):** 680-681.
23. Seyedmohammadi, J., Navidi, M. N. and Esmaeelnejad, L. 2019. Geospatial Modeling of Surface Soil Texture of Agricultural Land Using Fuzzy Logic, Geostatistics and GIS Techniques. *Commun. Soil Sci. Plant Anal.*, **50(12):** 1452-1464.
24. Shahriari, M., Delbari, M., Afrasiab, P. and Pahlavan-Rad, M. R. 2019. Predicting Regional Spatial Distribution of Soil Texture in Floodplains Using Remote Sensing Data: A Case of Southeastern Iran. *Catena*, **182:** 104149.
25. Tashayo, B., Honarbakhsh, A., Akbari, M. and Ostovari, Y. 2020. Digital Mapping of Philip Model Parameters for Prediction of Water Infiltration at the Watershed Scale in a Semi-Arid Region of Iran. *Geoderma Reg.*, **22**: e00301.
26. Turan, İ. D., Dengiz, O. and Özkan, B. 2019. Spatial Assessment and Mapping of Soil Quality Index for Desertification in the

[DOI: 10.52547/jast.25.2.485]

Semi-Arid Terrestrial Ecosystem Using MCDM in Interval Type-2 Fuzzy Environment. *Comput. Electron. Agric.*, **164:** 104933.

27. Vrbik, J. 2020. Deriving CDF of Kolmogorov-Smirnov Test Statistic. *Appl. Math.*, **11(3):** 227-246.

28. Xing-Yi, Z. S., Yue-Yu, Z., Xu-Dong, M., Kai, S. and Herbert, J. 2007. Spatial Variability of Nutrient Properties in Black Soil of Northeast China. *Pedosphere*, **17(1):** 19–29.

افزایش کیفیت نقشه های رقومی بافت خاک با استفاده از تصاویر ماهواره لندست ۸ در خاک های آهکی جنوب ایران

م. پوزش شیرازی، س. ع. ابطحی، م. باقر نژاد، س. ع. ا. موسوی، و م. ن. نویدی

چکیده

در طی سه دهه اخیر، تمایل عمومی به تغییر روش در تحقیقات پیرامون مدیریت منابع خاک و نقشه برداری اراضی از روش های مرسوم و عمدتاً کیفی به روش های کمّی بر اساس مدل های همبستگی مکانی بوجود آمده است که به این روش ها اصطلاحاً نقشه برداری رقومی خاک گفته می شود. پژوهش حاضر در دشت شبانکاره استان بوشهر به مساحت ۱۵۰۰۰ هکتار با واحدهای فیزیوگرافی مختلف که دارای کاربری عمدتاً زراعی بودند انجام شد. تعداد ۱۷۲ محل هدف برای نمونه برداری خاک در عمق ¬-۳۰-۰ سانتیمتری بر اساس تصاویر ماهواره ای و همچنین تفاوت¬های ظاهری مشاهده شده در منطقه مطالعاتی در نظر گرفته شد. نقشه رقومی بافت خاک به دو روش زیر تولید گردید (a :روش مرسوم و متداول در تهیه نقشه رقومی خاک. در این روش، نتایج به دست آمده از تجزیه¬ نمونه¬های خاک در آزمایشگاه را به¬همراه مختصات جغرافیایی هر نقطه و مرز منطقه مورد مطالعه به محیط برنامه رایانه¬ای ArcGIS وارد نموده و با استفاده از تخمین¬گرهای کریجینگ (Kriging) و یا عکس مجذور فاصله(IDW) ، نقشه مربوطه تهیه می شود. نقشه¬های تولید شده به این روش دارای کیفیت پایینی هستند به گونه ای که در آن ها علاوه بر بافت¬های موجود در خاک سطحی منطقه مطالعاتی، بافت¬های اضافی و پراکنده با مرزهای تیز و غیر واقعی نیز مشاهده می¬گردند (b .روش پیشرفته که از کوکریجینگ (CoKriging) باندهای انعکاسی سنجده OLI ماهواره لندست ۸ با نتایج آزمایشگاهی نمونه های خاک برای ترسیم نقشه بافت خاک استفاده می گردد. نتایج نشان داد که به کارگیری باند B1 (433/0 تا ۰/٤٥۳ میکرومتر) تصاویر ماهواره لندست ۸ مربوط به آوریل ۲۰۲۰ توانست بالاترین کیفیت در ترسیم نقشه رقومی بافت خاک منطقه مورد مطالعه را بوجود آورد. نقشه بافت خاک تولید شده در این روش با بافت خاک سطحی در طبیعت کاملاً مطابقت داشت. تجمع نمک و میزان رطوبت خاک از عوامل مهمی بودند که بر تاریخ تصویر ماهواره

[DOI: 10.52547/jast.25.2.485]

ای انتخاب شده، نقش عمده ای داشتند. همچنین، بیشترین و کمترین شعاع تأثیر در بین ذرات بافت خاک به ترتیب مربوط به ذرات رس و شن به میزان ٦٨٤ و ٣٨٨ متر بود.

[DOI: 10.52547/jast.25.2.485]